A Robust Response of Precipitation to Global Warming from CMIP5 Models

K.-M. LAU

Laboratory for Atmospheres, NASA, Goddard Space Flight Center, Greenbelt, MD.

H.-T. WU

Science Systems and Applications, Inc., Lanham, MD.

K.-M. KIM

Morgan State University, Baltimore, MD.

Correspondence to: Dr. William K.-M. Lau, Earth Science Division, Atmospheres, Code 613, Building 33, Rm C121, NASA Goddard Space Flight Center, Greenbelt, MD 20771, USA; email: William.K.Lau@nasa.gov

Abstract

How precipitation responds to global warming is a major concern to society and a challenge to climate change research. Based on analyses of rainfall probability distribution functions of 14 state-of-the-art climate models, we find a robust, canonical global rainfall response to a triple CO_2 warming scenario, featuring 100–250% more heavy rain, 5–10% less moderate rain, and 10–15% more very light or no-rain events. Regionally, a majority of the models project a consistent response with more heavy rain events over climatologically wet regions of the deep tropics, and more dry events over subtropical and tropical land areas. Results suggest that increased CO_2 emissions induce basic structural changes in global rain systems, increasing risks of severe floods and droughts in preferred geographic locations worldwide.

One of the key findings of the Fourth Assessment Report (AR4) of the Intergovernmental Panel on Climate Change (IPCC) is that "*anthropogenic influences have contributed to intensification of extreme precipitation at the global scale*" (*1*). The AR4 also noted that while climate models generally project a global increase in rainfall, the projected rate of change and regional signals are highly uncertain, due to coarse model resolution and inadequate model physics. In recent years, many record breaking extreme heavy rain, and prolonged heat waves and droughts events have been reported worldwide (*2*). This is consistent with a growing body of recent studies suggesting that there is an increased risk of extreme heavy rain events in a warmer climate (*3–9*). However the regional distribution of the increased extreme heavy rain and attribution to specific climate forcing are still uncertain. In preparation for the Fifth Assessment Report (AR5), IPCC has organized the Coupled Model Intercomparison Project Phase 5 (CMIP5), coordinating major international research institutions and groups to conduct climate model projection experiments under various emission scenarios (*10*). In this study, we assess CMIP5 model projections of global and regional rainfall response to greenhouse gases (GHG) warming, specifically to increased CO_2 emissions. Here, the focus is not only on extreme heavy rainfall, but also on the possible changes in rainfall characteristics (types, intensity and duration) by examining changes in the entire rainfall probability distribution function (PDF). The results presented in this paper are based on climate projection experiments from 14 CMIP5 models available at the time of this study. While the 14 models have diverse resolutions (table S1) and representations of physical, chemical, hydrological and oceanic processes, they are subject to the same set of prescribed GHG emission scenarios as specified by IPCC (*10*). Here, we analyze the outputs of 14 CMIP5 models based on a 140-year experiment with a prescribed

1% per year increase in CO_2 emission (1PPY) scenario. A 27-year period at the beginning of the IPPY integration is used as the control to compute rainfall and temperature statistics. Two similar 27-year periods in the 1PPY experiment that correspond approximately to a doubling of CO_2 emissions (DCO2) and a tripling of CO_2 emissions (TCO2) from the control are chosen respectively to compute the same statistics (see Methodology and Data in Supplementary Material). The responses to global warming are defined as the differences in the 27-year statistics between the control and DCO2, and TCO2 respectively. In addition, a 27-year period (1997–2005) in the historical run with prescribed sea surface temperature and GHG and aerosol emissions is used to evaluate the climatological rainfall statistics of each model, by comparing with rainfall data from the Global Precipitation Climatology Project (GPCP) and from the Tropical Rainfall Measuring Mission (TRMM) (see Table S1 in Supplementary Material). Results indicate that the temperature and rainfall responses in both DCO2 and TCO2 are qualitatively similar, except that the latter has higher signal-to-noise ratio, *i.e.*, larger magnitude response and smaller variability among models. For brevity, results presented in the main text are based mostly on TCO2.

Model rainfall climatology. The model climatology of zonal mean rainfall for each of the 14 CMIP5 models is compared to observations over the historical period 1979–2005. Overall, the zonal mean rainfall profiles of the CMIP5 models are in good agreement with observations (Fig. 1A). All models show the two off-equatorial peaks in the deep tropics between 5° and 10° latitudes, and two subtropical minima between 20° and 30° latitudes. The higher peak in the Northern Hemisphere (NH) reflects the stronger summer monsoon compared to its Southern Hemisphere (SH) counterpart. Most models overestimate the rain rate over the deep tropics,

especially over the SH. Given the model diversity, the overall agreement with observation is quite good.

The cumulative PDF (CPDF) of frequency of occurrence (FOC) and rain amount for all models and their ensemble mean, and for GPCP are computed over the near-global domain (60^oS—60^oN) (Fig 1B). Here it can be seen that the model ensemble CPDFs agree reasonably well with GPCP observations, but under-estimate the FOC at lower rain rates. To facilitate later discussions, we define based on the ensemble CPDFs, light rain (LR), moderate rain (MR), and heavy rain (HR) events as those with monthly mean rain rate in the range of 0.024 – 0.3 mm/day, 0.9 – 2.4 mm/day, and > 9 mm/day respectively. Previous studies have used similar classification of rain rate to identify with different physical characteristics of rain and cloud types (*5, 6, 11*). From Fig. 1B, LR occupies 5–25% of the total rain events, but only less than 5% of the total rain amount. MR contributes to 40–70% of the rain events, while accounting for a substantial portion (up to 40%) of the total rain amount. Most important, HR occurs only rarely (~1.5% of rain events), but contributes a significant amount (> ~ 10%) of the total rain amount. The FOC CPDFs show relatively large deviations about the ensemble mean for LR compared to HR. Conversely, the rain amount CPDFs show large deviations in HR compared to LR events. These reflect the large differences in representation of light rain in the CMIP5 models, and the large variations in rain physics and model resolution in simulating heavy rain events.

Changes in global and zonal mean temperature and rainfall. All models show a clear increase in global ($60^\circ S$–$60^\circ N$) mean temperature from the increased CO_2 emissions in 1PPY, with a rate of 0.2–0.36 K/decade among models, and an model ensemble mean of 0.26 K/decade (Fig. 2A). Similarly, all models exhibit a clear upward trend in the annual global mean precipitation with increasing CO_2 emissions, with a hint of faster increase for beyond Year 50–

80 (Fig. 2B). The ensemble-mean rate of global mean precipitation increase is about 0.012 mm/day/decade or 0.38% increase per decade.

In response to global warming under TCO2, most models show significant increase of rainfall in the deep tropics (10°S–10°N), and mid-to-high latitudes in both hemispheres (Fig. 2C). Concomitantly, reduced rainfall is found in the subtropics, more pronounced in the Southern than the Northern Hemisphere, although variability among models is quite large. The model ensemble response (Fig. 2D) shows three distinct zones of rainfall increase: 10°S–10°N, south of 45°S, and north of 40°N; and a wide rainfall-reduction zone near 10°S–40°S, and a near rainfall-neutral zone near 20°N–40°N. As shown in the Supplementary Material, the near neutral zone in NH subtropics may be an artifact of the zonal mean that masks large regional differences. Additional analyses of zonal mean profiles over selected longitudinal sectors (fig. S1 and supplementary text) show that there is a significant rainfall reduction in the NH subtropics over North America, and the Europe-Africa sectors, but increased rainfall over the subtropical central Pacific and Asian monsoon sectors. These regional rainfall anomalies compensate to produce in the zonal mean a near neutral zone over the NH subtropics (Fig. 2D). The rainfall anomalies are consistent with observations of an overall widening of the tropical belt in recent decades (*12–14*), with increased subsidence (reduced rainfall) over wider areas in the subtropics in both hemispheres, but with strong east-west asymmetry. More detailed discussion of regions of reduced rainfall with respect to the geographic distribution of prolonged droughts is presented later.

While CO_2 warming is the root cause of the increase in global rainfall by the experimental design, it is clear from the changes in zonal profiles of rainfall shown above that the response of rainfall to global warming is dependent not only on temperature, but on remote

forcing, and local dynamical feedbacks (*5, 15*). Even though there is overall warming (+3.7 K) globally, the temperature response in TCO2 is by no means uniform (Table 1). Faster rate of temperature increase is found in the NH as expected from the higher land-to-ocean ratio and higher population density and anthropogenic activities compared to the SH. The accelerated temperature increase in northern polar latitudes (+6.2 K) is consistent with increased ice-albedo feedback (*16*). Similarly, zonal mean rainfall response varies greatly by latitudes, including a change in sign, ranging from +18.8% in northern polar region to -2.4% in the SH subtropics. Globally, rainfall increases by 5.7%, with a sensitivity (dP/P/dT) of 1.6% K^{-1}(Table 1), significantly lower than the 7% K^{-1} increase in saturated water vapor governed by the Clausius-Clapeyron relation. The implication of this on a weakening of the tropical circulation has been reported (*17, 18*), but is outside the scope of this study. The highest sensitivity of rainfall to temperature is found over southern mid-to-high-latitudes (50–80°S), with a value of +6.3% K^{-1} (Table 1). The northern mid-to-high-latitudes (50–80°N) and the equatorial region (10°S–10°N) also show significant (+3% K^{-1}) sensitivity. Negative temperature sensitivity is found over the NH subtropics, SH subtropics and mid-latitudes, suggesting the importance of large-scale circulation forcing (see also discussion related to Fig. 2).

Changes in rainfall characteristics. The changes in rainfall characteristics in TCO2 are analyzed based on an examination of the ensemble mean of the monthly rainfall PDFs, and their differences (Fig. 3A). The mean PDFs (line graphs in logarithmic scale) show that clearly there is a tendency for increase in extreme heavy rain events globally due to CO2 warming. However, the logarithmic scale in the mean PDF plot masks changes in lower rain rates. The linear difference PDF plot (Fig. 3A, bar chart) provides a different perspective, displaying a

consistent and robust model response to CO_2 warming, with more HR, less MR and more LR. While there are variations among models in the magnitudes and exact thresholds rain rates at which the response changes sign, the shift pattern in the manner of a "flattening" of rainfall PDFs agree well among all models. Following Lau and Wu (*5, 6*), we normalize the absolute changes in FOC with respect to the control for each rain bin to highlight the heavy rain events (Fig. 3B). Here, a canonical shift pattern in response to CO_2 warming is evident, *i.e., increasing sensitivity of heavy rain, a decrease in moderate rain, and increase in light rain*. For extreme heavy rain events (e.g. monthly rainrate > 24 mm/day), the corresponding ensemble mean change is 100%–250% increase in rain amount. For MR and LR, the changes are approximately 10–15% and 5–10% respectively. We have also carried out analyses of the GHG-induced changes of rain PDFs over land and over ocean separately, and for different latitudinal zones. Results (fig. S2 and supplementary text) show that as long as sufficiently large domains are chosen, the canonical pattern of rainfall redistribution emerges. Comparing results for different CO_2 emissions rates, the magnitude of the canonical rainfall response in the major rain types have almost doubled from DCO2 to TCO2 (Table 2). Most noteworthy, the extreme heavy rain events have increased dramatically from 86.4% to 339% between those two periods. This indicates that the canonical response is highly nonlinear and scale selective, with the most heavy rain events increasing at a much faster rate than the rate of increase of CO_2 emissions.

Geographical distributions of rain types. To examine the common features in the geographic distribution of rainfall responses among the 14 CMIP5 model, we interpolate all model outputs to a common (1.125 longitude x 1.07 latitude; 320 x 192 grids) resolution. We further define a consistency number at each grid point, as the number of models showing the same positive or

negative sign in rainfall response at that grid point in TCO2. In Fig. 4, a grid-point ensemble value is defined only if the corresponding consistency number is 10 or larger, *i.e*., only when more than two third of the models show the same sign of response. Geographic distributions are shown for the ensemble mean response in terms of changes in annual amount for total rain, for HR, MR and LR respectively. There is a large increase in total rain in climatologically wet regions of the tropics, particularly, the Pacific ITCZ, the Asian monsoon regions including the equatorial India Ocean, South and Southeast Asia, and the maritime continent (Fig. 4A). Rainfall is also moderately increased over the extratropics of both hemispheres, poleward of 50^{o} latitude. A general reduction of rainfall is found in the climatologically dry subtropical oceans, as well as in land regions of Central America and southwestern US, southern Europe/Mediterranean, and South Africa. As a result, North America exhibits a dipole like anomaly pattern with reduced (enhanced) rainfall over the southern (northern) part of the continent. A similar but weaker dipole pattern is found over southern and northern Europe. As shown in Fig. 4B, most of the increased rainfall in the tropics is contributed by HR. Particularly pronounced is the increased HR over the Asian monsoon region and the Pacific ITCZ. Increased HR is also noted over coastal regions of extratropical North America and East Asia. Most interestingly, very few regions experience a reduction in HR anywhere in the globe. This is akin to the outcome of throwing a loaded dice with heavy odds in favor of increased HR events due to global warming.

In contrast to HR, there is an overall reduction in MR over extensive regions in the subtropical and midlatitude oceans (Fig. 4C). Interestingly, significant increase of MR is found over extratropical land regions of North America and Eurasia, as well as high-latitudes (>50°S) of the Southern Oceans. LR (Fig. 4D) has a distribution similar but with opposite signs to those

of MR. The presence of many regions where that are collocated responses in HR, MR and/or LR with different signs may be indicative of change in the vertical structure of hydrometeors and clouds in rain bearing systems over the regions (5).

Increased risk of drought. Here, we point out that the monthly mean rain-rate at a grid box used to construct the rainfall PDF does not represent an instantaneous rain event, but rather an unconditional (including no rain) mean of events of different rain rates over a monthly period. Since models seldom produce absolutely no rain over a month period at any grid point due to inadequate physical representation, the first two rain bins (monthly rain rate < 0.024 mm/day) in the rainfall PDF (Fig. 2) represent either no rain, or trace amount of rain. The occurrence of such an event at each grid location will be hereafter referred to as a "dry month" for that location. Using this definition, dry months occur about 3–10 % (ensemble mean = 5%) of the time anywhere in the global during the 27-year control period, but with negligible contribution to the rain amount (Fig. 1B). Under TCO2, the total number of dry months in the ensemble mean increases by 16 % (Fig. 3B). The increase in dry months occurs predominantly over land areas in the subtropics or marginal convective zones at the edge of climatological wet zones in both hemispheres (Fig. 5). The spatial distribution suggests some degree of coupling between the NH and SH through an anomalous meridional circulation with rising motion over the deep tropics and subsidence over the dry zones, but strongly constrained by the geography of the major continents. Over the Euro-Africa continent, the model ensemble projects a pronounced increase in dry months over a long and narrow east-west zone extending from North Africa/Mediterranean/Southern Europe to Iran, and over southern Africa. Over the American continent, more dry months are found in Southwestern US/Mexico region, and northeastern

Brazil. Much weaker dry zones are found over Southeast Asia and southern Australia. The dry regions generally coincide with reduced rainfall zones in the total rainfall distribution shown in Fig. 4A. Because of the positive-definite nature of rainfall, a prolonged period of no rain in climatologically dry regions will not show up as a major anomaly in a rainfall map (Fig. 4), but will be captured in a map of dry month distribution (Fig. 5). Hence, regions shown in Fig. 5 could be interpreted as those that will have high risk of experiencing longer dry months or drought–like conditions under TCO2. Interestingly, CMIP5 models project no spatially coherent reduction in dry months anywhere in the globe under TCO2, again analogous to the outcome of throwing a loaded dice with overwhelming odds in favor of increased droughts due to global warming.

Summary and Discussion. The IPCC CMIP5 models project a robust, canonical global response of rainfall characteristics to CO_2 warming, featuring an increase in heavy rain, a reduction in moderate rain, and an increase in light rain occurrence and amount globally. For a 1% increase per year scenario, the model ensemble mean projects, at the time of approximately tripling of the CO2 emissions, the probability of occurring of extremely heavy rain (monthly mean > 24 mm/day) anywhere in the global will increase by 100–250%, moderate rain will decrease by 5–10% and very light and no-rain events will increases by 10–15%. The increase in heavy rain is most pronounced in the Pacific ITCZ and the Asian monsoon regions. Moderate rain is reduced over extensive oceanic regions in the subtropics and extratropics, but increased over the extratropical land regions of North America, and Eurasia, and extratropical Southern Oceans. Light rain is found inversely related to moderate rain locally, and with heavy rain in the central Pacific. The model ensemble also projects a significant increase up to 16% more frequent in the

occurrence of dry months (drought conditions) globally, mostly over subtropical, and marginal convective zone in equatorial land regions. The most pronounced drought-like signal is found over a east-west fetch spanning North Africa, Mediterranean Sea, Southern Europe to Iran, and another one over southern Africa. A secondary region of increased risk of drought is found over Southwest US/Mexico, and northeastern Brazil. A much weaker drought-prone region is found over Southeast Asia, and southern Australia. The propensity for prolonged dry months over tropical regions and marginal tropical convective zones over large landmasses suggests the importance of land-atmosphere feedback in leading to severe droughts (*19*).

With the aid of satellite data, light, moderate and heavy rain types have been identified with rainfall characteristics in terms of convection types associated with warm rain/low clouds, mixed-phase rain/congestus, and ice-phase rain/high clouds respectively (*5, 6, 11*). The canonical pattern of rainfall response to CO2 warming captured in the CMIP5 model projection suggests a global scale re-adjustment involving changes in rainfall characteristics, as well as possible linkage of extremely heavy rain and droughts in different parts of the globe. This connection is possibly effected through adjustments of the large scale circulation in response to global warming (*20*). This adjustments are strongly constrained by the climatological rainfall pattern, *i.e.*, monsoon and desert distributions, and is consistent with the rich-getting-richer-and-poor-getting-poorer economic paradigm (*21, 22, 5, 14*). It is also in agreement with observations of increased rainfall in the deep tropics, drying and expanding of the subtropical dry zones, as well as the notion of more frequent occurrence of regional rainfall extremes and prolonged drought events in recent decades (*23–26, 4, 12, 13*). To better understand the causes and consequences of changes in regional rainfall in response to global warming, more work is needed to analyze in further details the nature of the climate forcing not only from greenhouse gases, but

also from local and regional forcing such as aerosols, land use and land change, and dynamical feedback processes from climate models simulations and observations.

References and Notes:

1. IPCC, *Climate Change 2007: The Physical Science Basis. Contribution of Working Group I to the Fourth Assessment Report of the Intergovernmental Panel on Climate Change*. S. Solomon *et al.*, Eds., (Cambridge University Press, Cambridge, United Kingdom, and New York, NY, USA, 2007), 996 pp.
2. C. B. Field *et al.*, Eds., *Managing the Risks of Extreme Events and Disasters to Advance Climate Change Adaptation: Special Report of the Intergovernmental Panel on Climate Change.* (2012).
3. R. P. Allan, B. J. Soden, V. O. John, W. Ingram, P. Good, *Environ. Res. Letters* **5**, (2010).
4. P. Ya. Groisman *et al.*, *J. Climate* **18**, 1326-1350 (2005).
5. K.-M. Lau, H.-T. Wu, *J. Geophys. Res.* **116**, D17111, 10pp. (2011).
6. K.-M. Lau, H.-T. Wu, *Int. J. Climatology* **27**, 979–988 (2007).
7. C. Liu, R. P. Allan, G. J. Huffman, *Geophys. Res. Lett.*, in press (2012).
8. S. K. Min, X. Zhang, F. W. Zwiers, G. C. Hegerl, *Nature* **470**, 378–381 (2011).
9. P. A. O'Gorman, T. Schneider, *Proceedings of the National Academy of Sciences* **106**, 14773–14777 (2009).
10. K. E. Taylor, R. J. Stouffer, G. A. Meehl 2012, *Bulletin of the American Meteorological Society* **93**, 485–498 (2012).
11. H. Masunaga, C. D. Kummerow, *Geophy. Res. Lett. **33***, L16805 (2006).
12. D. J. Seidel, Q. Fu, W. J. Randel, T. J. Reichler, *Nat. Geosci*., **1**, 21–24 (2008).
13. Y. Hu, Q. Fu, *Atmos. Chem. Phys.* **7**, 5229–5236 (2007).
14. Y. P. Zhou, K. M. Xu, Y. C. Sud, A. K. Betts, *J. Geophys. Res.* **116**, D09101 (2011).
15. C. Chou, C.-A. Chen, P.-H. Tan, K.-T. Chen, *J. Climate* **25**, 3291–3306 (2012).

16. J. A. Curry, J. Schramm, E. E. Ebert, *J. Climate*, **8**, 240–247 (1995).

17. I. M. Held, B. J. Soden, *J. Climate* **19**, 5686–5699 (2006).

18. G. A.Vecchi *et al*., *Nature* **441**, 73–76 (2006).

19. K. L. Brubaker, D. Entekhabi, *Water Resource Res*. **32**, 1343–1357 (1996).

20. K.-M. Lau, K-M. Kim K-M, *J. Hydromet.* **13**, 392–403 (2012).

21. C. Chou, J. D. Neelin, *J. Climatol.* **17**, 2688–2701 (2004).

22. C. Chou, J. D. Neelin, C. A. Chen, J. Y. Tu, *J. Clim.* **22**, 1982–2005 (2009).

23. B. N. Goswami, V. Venugopal. D. Sengupta, M. S. Madhusoodanan, P. K. Xavier, *Science* **314**, 1442–1445 (2006).

24. J. Lu, C. Deser, T. Reichler, *Geophys. Res. Lett*. **36**, L03803 (2009).

25. R. Seager *et al*., *Science* **316**, 1181–1184 (2007).

26. X. Zhang *et al*., *Nature* **448**, 461–465 (2007).

Acknowledgements: This work is funded by the Precipitation Measurement Missions (PMM) and the Modeling and Analysis Program (MAP), NASA Headquarters.

The CMIP5 data is available through the Earth System Grid - Center for Enabling Technologies (ESG-CET), on the page http://pcmdi9.llnl.gov/. The primary website for the GPCP Version 2 monthly Satellite-Gauge (SG) the World Meteorological Organization's World Data Center at NOAA's National Climatic Data Center. The TRMM Multi-Satellite Precipitation Analysis (TMPA; computed at monthly intervals as 3B-43) is available through the TRMM data access page, which is located at NASA's Goddard DAAC.

Table 1. CO_2 warming induced changes in mean rain rate (dP/P) and mean surface temperature (dT), and sensitivity (dP/P/dT) at different latitudinal zones under TCO2.

Latitude Range	*(80°S – 80°N)*	*(80°S – 50°S)*	*(50°S – 30°S)*	*(30°S – 10°S)*	*(10°S – 10°N)*	*(10°N – 30°N)*	*(30°N – 50°N)*	*(50°N – 80°N)*
dP/P	+5.7%	+17.6%	-1.2%	-2.4%	+9.9%	-0.39%	+3.5%	+18.8%
dT (K)	3.7	2.8	2.0	3.1	3.3	3.5	4.0	6.2
dP/P/dT (%/K)	+1.6	+6.3	-0.6	-0.8	+3.0	-0.1	0.87	+3.0

Table 2. CO_2 warming induced changes in fractional precipitation (dP/P) for different rain types.

Rain types	*ALL*	*Extreme Heavy*	*Heavy (HR)*	*Moderate (MR)*	*Light (LR)*
DCO2	2.45 %	86.4 %	13.6 %	-4.70 %	3.48 %
TCO2	4.48 %	339 %	23.2 %	-8.35 %	6.0 %

Figure legends:

Fig. 1. Rainfall climatology of historical run form each of the 14 CMIP models, and rainfall observations (GPCP) for the period 1979–2005. (A) Zonal mean rain rate, and (B) cumulative probability distribution functions (CPDF) of rain occurrence and amount for each model and for GPCP. Rainfall climatology from TRMM observations for the period 1998–2011 are also shown in (A).

Fig. 2. Changes in annual global (60°S–60°N) mean for (A) surface temperature and (B) rainfall in the IPPY run from Year 1 to Year 140; (C) the difference in the zonal mean rain rate of the control and in TCO2 from each of the 14 CMIP5 models; and (D) the ensemble mean zonal mean rain rates of the control (blue) and TCO2 (red), and their difference.

Fig. 3. Response in precipitation to global warming in TCO2 scenario as a function of rain rate: (A) change in the frequency of occurrence (FOC) and (B) normalized change in rain amount. Response of each of the 14 CMIP5 models is denoted by different color marks, and the model ensemble mean is denoted by the bar chart. Also shown in (A) are the ensemble mean FOC of the control and TCO2 (solid curves), scaled by log 10.

Fig. 4. Geographic distribution of the ensemble-mean rainfall response in TCO2, in terms of changes in annual mean amount (mm/year) for (A) total rain, (B) heavy rain, (C) moderate rain, and (D) light rain. Only regions with high consistency (*i.e*. responses of 10 or more out of the 14 models are of the same sign) are shown.

Fig. 5. Geographic distribution of the ensemble-mean response in TCO2 scenario in terms of the changes in the number of dry months per year. Only regions with high consistency (responses of 10 or more out of the 14 models are of the same sign) are shaded. Superimposed is the ensemble-mean precipitation (in mm/day) for the control period in contour lines.

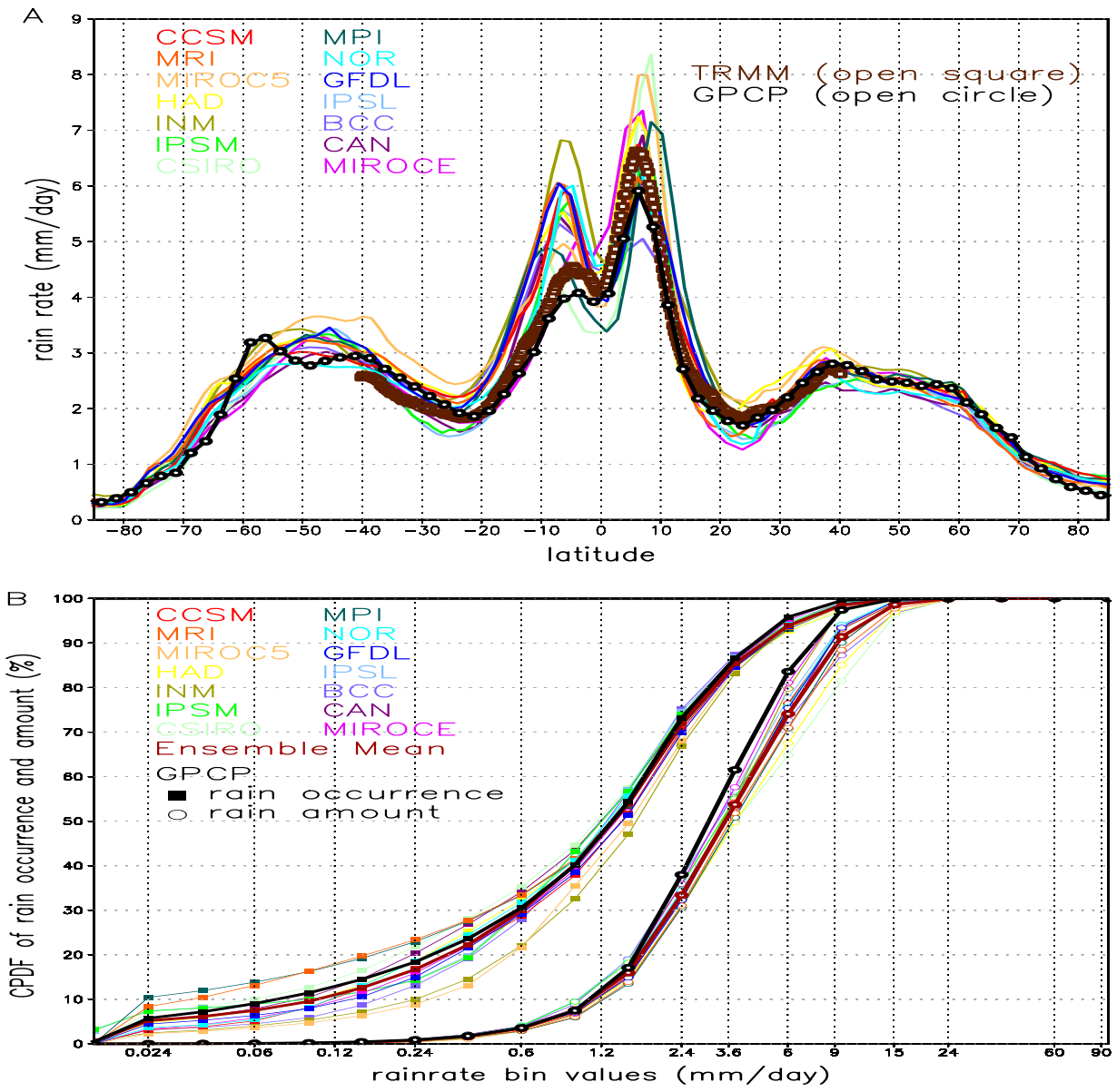

Fig. 1. Rainfall climatology of historical run form each of the 14 CMIP models, and rainfall observations (GPCP) for the period 1979–2005. (A) Zonal mean rain rate, and (B) cumulative probability distribution functions (CPDF) of rain occurrences and amount. Rainfall climatology from TRMM observations for the period 1998–2011 are also shown in (A).

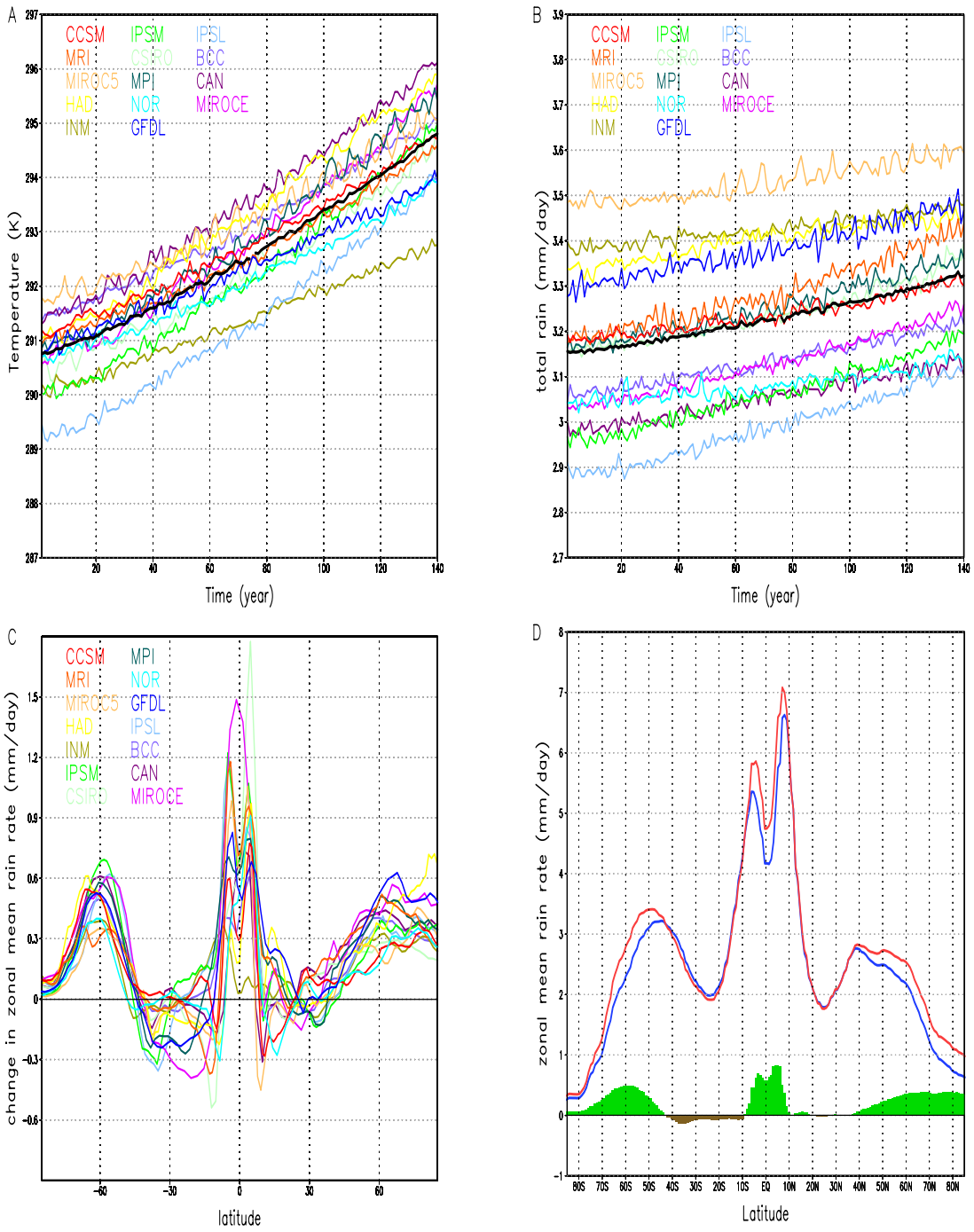

Fig. 2. Changes in annual global (60°S–60°N) mean for (A) surface temperature and (B) rainfall in the IPPY run from Year 1 to Year 140; (C) the difference in the zonal mean rain rate of the control and in TCO2 from each of the 14 CMIP5 models; and (D) the ensemble mean zonal mean rain rates of the control (blue) and TCO2 (red), and their difference.

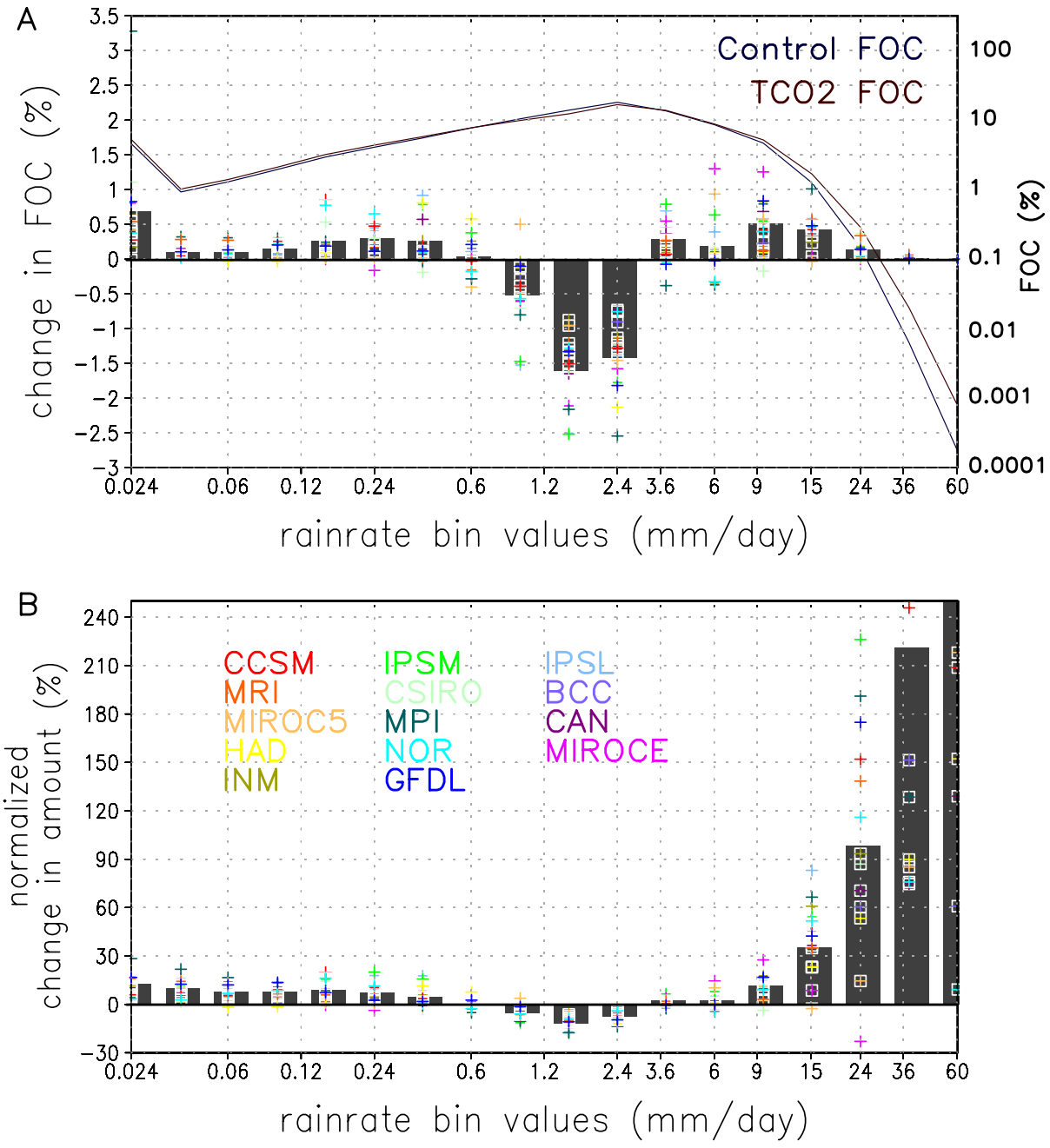

Fig. 3. Response in precipitation to global warming in TCO2 scenario as a function of rain rate: (A) change in the frequency of occurrence (FOC) and (B) normalized change in rain amount. Response of each of the 14 CMIP5 models is denoted by different color marks, and the model ensemble mean is denoted by the bar chart. Also shown in (A) are the ensemble mean FOC of the control and TCO2 of the IPPY run (solid curves), scaled by log 10.

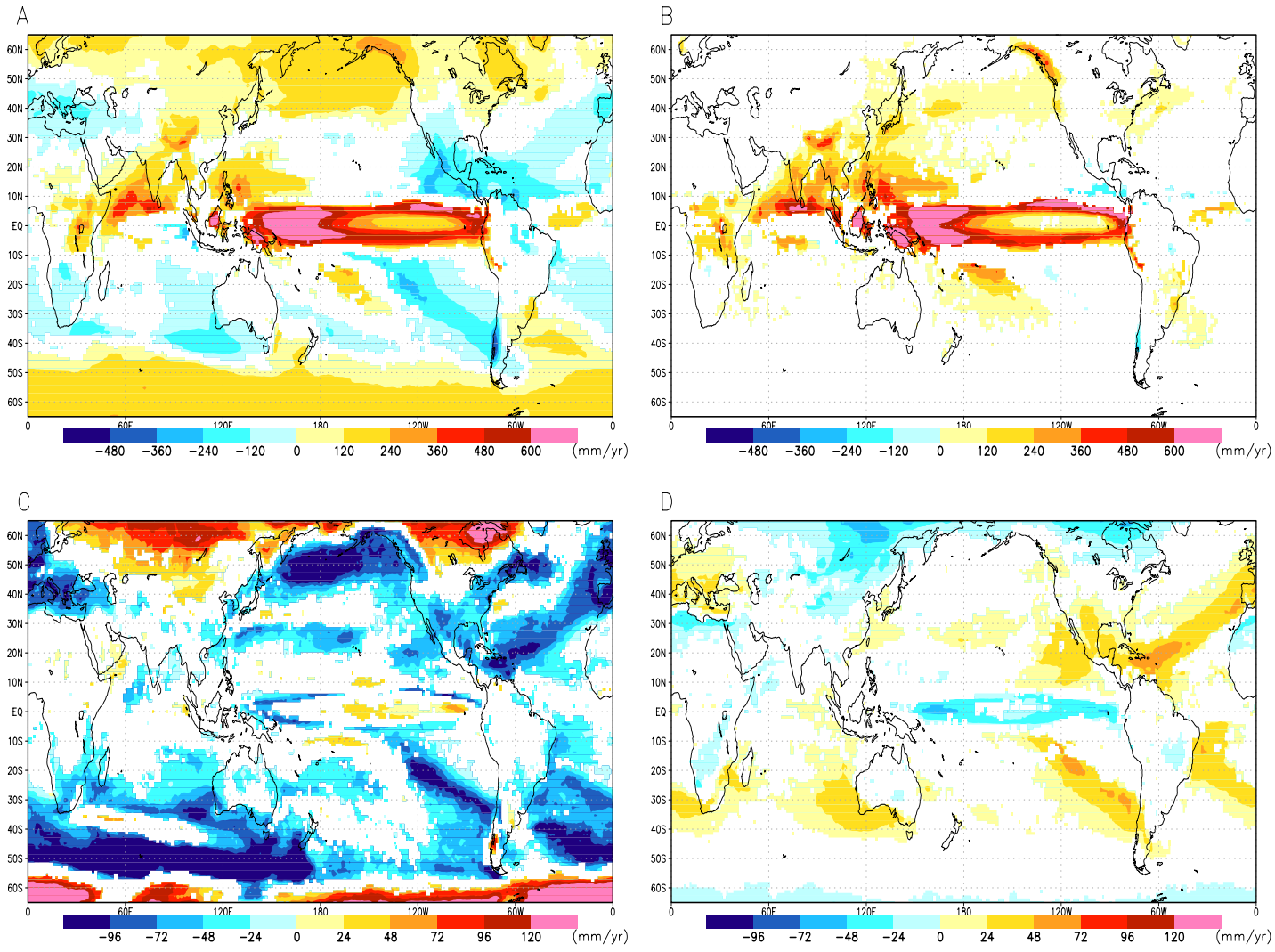

Fig. 4. Geographic distribution of the ensemble-mean rainfall response in TCO2 scenario in terms of changes in annual mean amount (mm/year) for (A) total rain, (B) heavy rain, (C) moderate rain, and (D) light rain. Only regions with high consistency (*i.e.* responses of 10 or more out of the 14 models are of the same sign) are shaded.

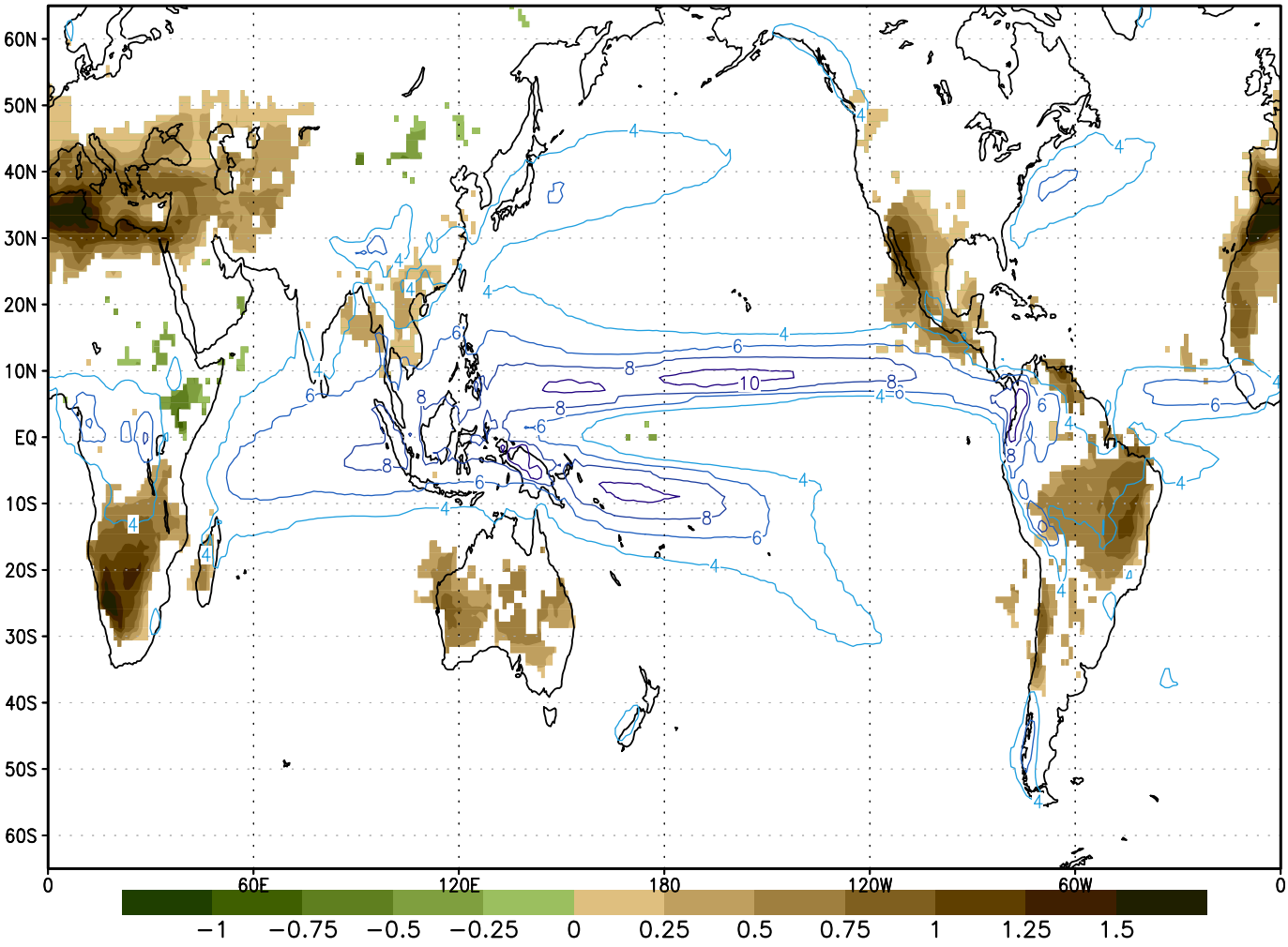

Fig. 5. Geographic distribution of the ensemble-mean response in TCO2 scenario in terms of the changes in the number of dry months per year. Only regions with high consistency (responses of 10 or more out of the 14 models are of the same sign) are shaded. Superimposed is the ensemble-mean precipitation (in mm/day) for the control period in contour lines.

Supplementary Materials:

Supplementary Text

Figs. S1 and S2

Table S1

References (*27–30*)

Methodology and Data. Probability distribution functions (PDF) of rainfall as a function of binned rain rates based on monthly data for are computed for each model and for the ensemble model mean to characterize the response in precipitation to GHG warming. We adopt the methodology used by Lau and Wu (*5, 6*) to evaluate the absolute and normalized rainfall changes as a function of binned rain rate in a warming climate. This methodology is analogous to the quantile regression analysis used to identify relationships among variables with respect to a predictor in case where there is no, or only weak relationship in the means of such variables to the predictor (*27, 28*). In the present context, the variables are light, moderate and heavy rains as characterized by binned rain rates. The predictor or change agent is the increased CO_2 emissions, by the experimental design. For validation of model rainfall climatology, we chose a common 27-year period (1979–2005) from the model's historical run (with prescribed sea surface temperature and GHG and aerosol emissions) and compare with the improved version of the longest available Global Precipitation Climatology Project (GPCP) monthly global rainfall observations (*29*). The Tropical Rainfall Measuring Mission (TRMM) rainfall products (*30*) for the same period are also used for additional crosscheck.

The responses of the rainfall PDF are examined under a scenario of 1% per year (1PPY) increment in CO_2 mission starting from pre-industrial conditions. The control rainfall and temperature

statistics are defined for the first 27-year (Year 1–27) period of the integration. Under 1PPY increment, the CO2 emissions would be nearly doubled in Year 70, and quadrupled by Year 140. The 27-year period (Year 71–97) in the middle of the 1PPY run corresponds approximately to a doubling of CO_2 emissions of the control period. Similarly, the last 27-year period (Year 114–140) of the 1PPY run corresponds approximately to a tripling of CO_2 emissions of the control period. Differences in rainfall and temperature statistics between the mid 27 years and the control, and those between the last 27 years and the control, will be referred to as the "response" to a double CO2 (DCO2), and the triple CO2 (TCO2) scenario respectively.

Zonal mean rainfall response at different longitude sectors. The net response of the zonal mean rain rate as a function of latitudes in four longitudinal sectors: Central Pacific (140°E–130°W), Americas (40–130°W), Africa (40°W–50°E), and (50–140°E) (Euro-Asia, Australia, Indian, and west Pacific) are depicted in Fig. S1A–D. All sectors exhibit increased rainfall with the strongest signal in the near equatorial regions (10°S–10°N), and secondary maxima in the extratropics (> 40–50° latitudes) of both hemispheres. A subtropical zone with reduced rainfall is found in each hemisphere in the American sector (Fig. S1B) and in the Western Europe/Africa sector (Fig. S1C). Over the Asian monsoon sector (Fig. S1D), only one subtropical drier zone is found in the southern hemisphere. The latitude profiles are consistent with an overall increase in the upward branch of Hadley circulation, and increased subsidence suppressing rainfall in the subtropics over the Americas and the Western Europe/Africa sectors. Under TCO2, the Asian monsoon appears to be enhanced, consistent with rising motion over NH monsoon land, and compensation subsidence over southern Australia. The reduced rainfall zone is also consistent with the prolonged dry months found over subtropical land regions (See Fig. 5 in main text).

Regional rainfall PDFs. The canonical response pattern of rainfall PDF to global warming, *i.e*., more HR, less MR and more LR, is captured in the land-only and ocean-only analysis respectively (Fig. S2A). Generally, the signal is stronger over ocean than over land. However, over land the increase in dry months (rain rate < 0.024 mm/day) is much more pronounced compared to ocean as shown in the upper panel of Fig. S2A, consistent with the discussion on dry months and droughts in the main text). Analyses of change in rainfall PDF have also been carried out, separately for the deep tropics (10°S–10°N) and for high-latitudes (50°–70° S and N, respectively), where there are substantial increases in total rainfall in TCO2 (see Fig. 2D in main text). Again, the canonical rainfall pattern emerges in all cases, with strongest signal in the deep tropics, followed by that in the NH, and the SH extra-tropics. In the deep tropics, and the extra-tropical NH land regions, the increase in the most intense rain events (monthly mean > 60 mm/day) could be up to 500% (lower panel of Fig. S2B).

Figure legends S1 and S2

Figure S1. As in Fig. 2D, but latitudinal zonal mean rainfall response under TCO2 for different meridional regions: (**A**) (140–230°E) central Pacific; (**B**) (40–130°W) America & surrounding oceans; (**C**) (40°W–50°E) Africa; and (**D**) (50–140°E) Euro-Asia, Australia, Indian and west Pacific Oceans.

Figure S2. As in Fig. 3, except showing separate analyses of different geographic regimes, with (**A**) illustrating change over land vs. change over ocean; and (**B**) illustrating change over deep tropics vs. change over high-latitudes.

Table S1. List of CMIP5 models and observational data sets analyzed in this study.

Model name	**Resolution (Lat x Lon)**	**Country/Center**
BCC-CSM1.1	**2.79° x 2.81°**	**China/BCC**
CanESM2	**2.79° x 2.81°**	**Canada/CCCma**
CCSM4	**0.94° x 1.25°**	**USA/NCAR**
CSIRO-Mk3.6	**1.86° x 1.88°**	**Australia/CSIRO**
GFDL-CM3	**2.02° x 2.50°**	**USA/NOAA**
HadGEM2-ES	**1.25° x 1.88°**	**United Kingdom/MOHC**
INM-CM4	**1.50° x 2.00°**	**Russia/INM**
IPSL-CM5A-LR	**1.89° x 3.75°**	**France/IPSL**
IPSL-CM5A-MR	**1.27° x 2.50°**	**France/IPSL**
MIROC5	**1.40° x 1.40°**	**Japan/MIROC**
MIROC-ESM	**2.79° x 2.81°**	**Japan/MIROC**
MPI-ESM-LR	**1.86° x 1.88°**	**Germany/MPI**
MRI-CGCM3	**1.11° x 1.13°**	**Japan/MRI**
NorESM1-M	**1.89° x 2.50°**	**Norwegian/NCC**
Observation	**Resolution (Lat x Lon)**	**Data Type**
GPCP v2.2 (1979–2005)	**2.50° x 2.50°**	**Merged Satellite-Gauge products**
TRMM 3B43 v7 (1998–2011)	**0.25° x 0.25°**	**Merged Satellite-Gauge products**

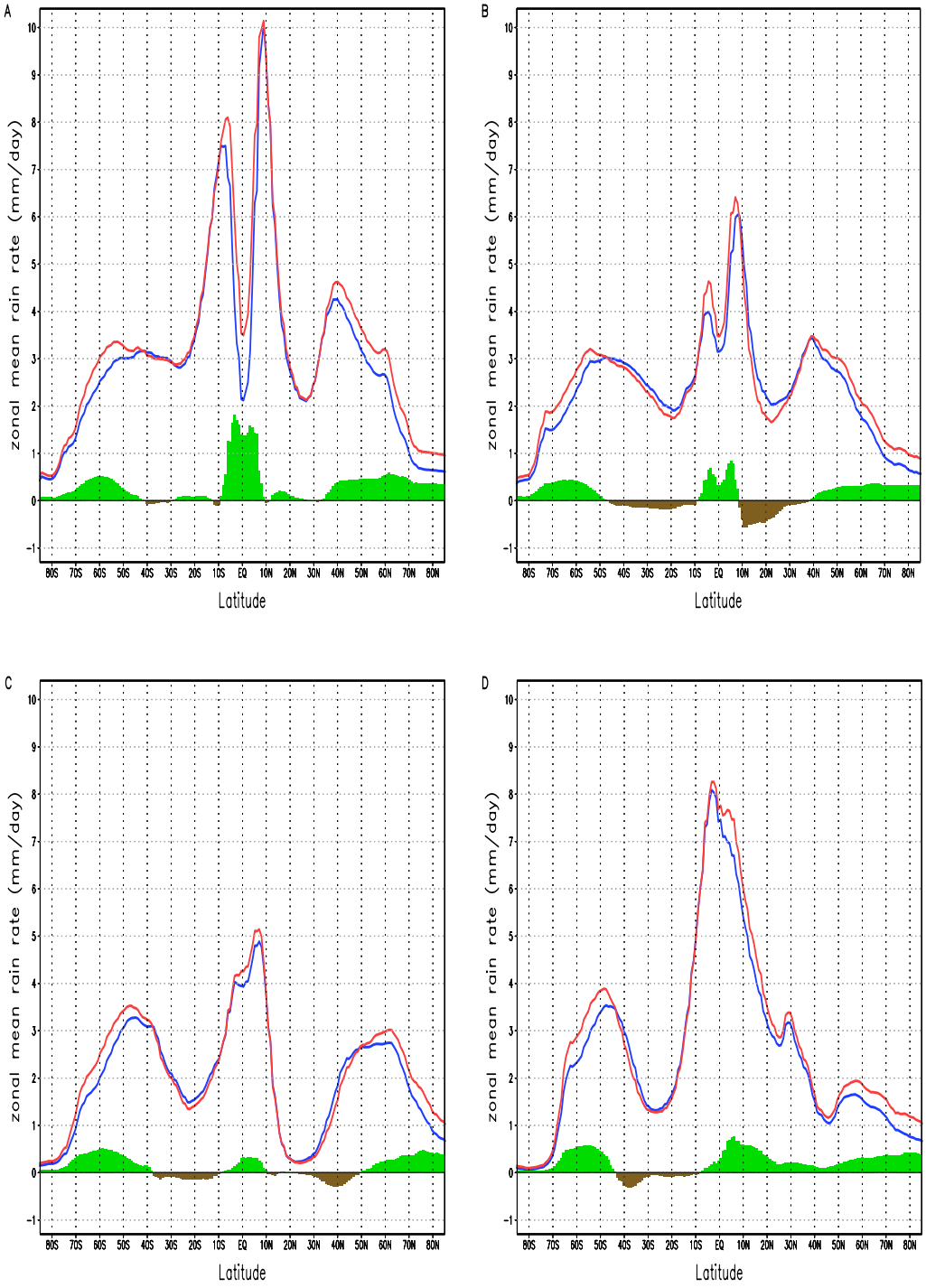

Figure S1. As in Fig. 2D, but latitudinal zonal mean rainfall response under TCO2 for different meridional regions: (**A**) (140–230°E) central Pacific; (**B**) (40–130°W) America & surrounding oceans; (**C**) (40°W–50E) Africa; and (**D**) (50–140°E) Euro-Asia, Australia, Indian and west Pacific Oceans.

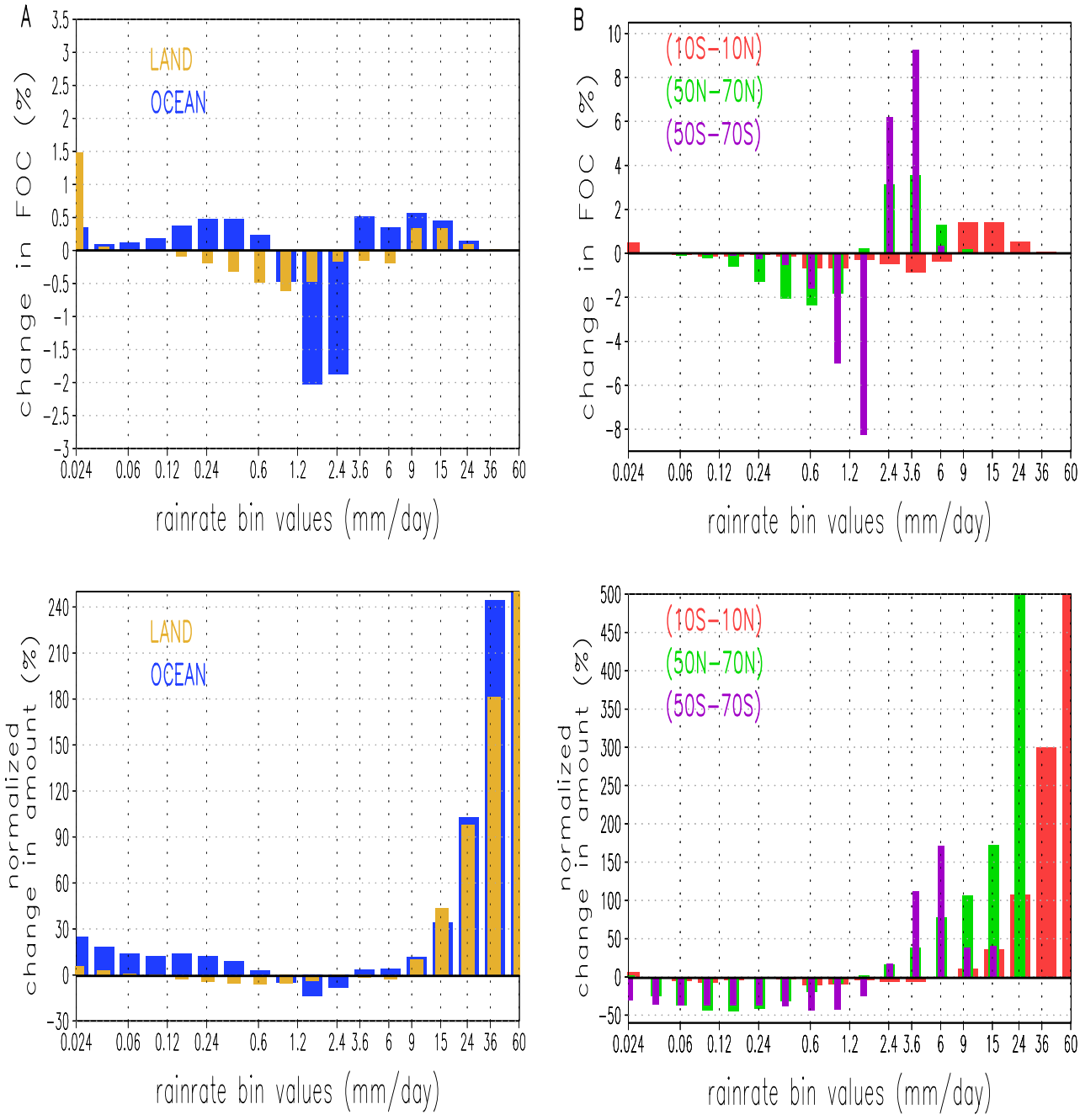

Figure S2. As in Fig. 3, except showing separate analyses of different geographic regimes, with (**A**) illustrating change over land vs. change over ocean; and (**B**) illustrating change over deep tropics vs. change over high-latitudes.

References and Notes:

1. IPCC, *Climate Change 2007: The Physical Science Basis. Contribution of Working Group I to the Fourth Assessment Report of the Intergovernmental Panel on Climate Change*. S. Solomon *et al.*, Eds., (Cambridge University Press, Cambridge, United Kingdom, and New York, NY, USA, 2007), 996 pp.
2. C. B. Field *et al.*, Eds., *Managing the Risks of Extreme Events and Disasters to Advance Climate Change Adaptation: Special Report of the Intergovernmental Panel on Climate Change.* (2012). http://ipcc-wg2.gov/SREX/ images/uploads/SREX-SPMbrochure_FINAL.pdf
3. R. P. Allan, B. J. Soden, V. O. John, W. Ingram, P. Good, Current changes in tropical precipitation. *Environ. Res. Letters* **5**, (2010). doi:10.1088/1748-9326/5/52/025205
4. P. Ya. Groisman *et al.*, Trends in intense precipitation in the climate record. *J. Climate* **18**, 1326-1350 (2005).
5. K.-M. Lau, H.-T. Wu, Climatology and changes in tropical oceanic rainfall characteristics inferred from Tropical Rainfall Measuring Mission (TRMM) data (1998–2009). *J. Geophys. Res.* **116**, D17111, 10pp. (2011). doi:10.1029/2011JD015827
6. K.-M. Lau, H.-T. Wu, Detecting trends in tropical rainfall characteristics, 1979–2003. *Int. J. Climatology* **27**, 979–988 (2007).
7. C. Liu, R. P. Allan, G. J. Huffman, Co-variation of temperature and precipitation in CMIP5 models and satellite observations. *Geophys. Res. Lett.*, in press (2012), doi:10.1029/2012GL052093
8. S. K. Min, X. Zhang, F. W. Zwiers, G. C. Hegerl, Human contribution to more intense precipitation extremes. *Nature* **470**, 378–381 (2011).

9. P. A. O'Gorman, T. Schneider, The physical basis for increases in precipitation extremes in simulations of 21st-century climate change. *Proceedings of the National Academy of Sciences* **106**, 14773–14777 (2009).

10. K. E. Taylor, R. J. Stouffer, G. A. Meehl 2012, An overview of CMIP5 and the experiment design. *Bulletin of the American Meteorological Society* **93**, 485–498 (2012). doi:10.1175/BAMS-D-11-00094.1

11. H. Masunaga, C. D. Kummerow, Observations of tropical precipitating clouds ranging from shallow to deep convective systems. *Geophy. Res. Lett.* ***33***, L16805 (2006). doi: 10.1029/2006GL026547

12. D. J. Seidel, Q. Fu, W. J. Randel, T. J. Reichler, Widening of the tropical belt in a changing climate, *Nat. Geosci*., **1**, 21–24 (2008).

13. Y. Hu, Q. Fu, Observed poleward expansion of the Hadley circulation since 1979. *Atmos. Chem. Phys.* **7**, 5229–5236 (2007). doi:10.5194/ acp-7-5229-2007

14. Y. P. Zhou, K. M. Xu, Y. C. Sud, A. K. Betts, Recent trends of the tropical hydrological cycle inferred from Global Precipitation Climatology Project and International Satellite Cloud Climatology Project data. *J. Geophys. Res.* **116**, D09101 (2011). doi:10.1029/2010JD015197

15. C. Chou, C.-A. Chen, P.-H. Tan, K.-T. Chen, Mechanisms for global warming impacts on precipitation frequency and intensity. *J. Climate* **25**, 3291–3306 (2012).

16. J. A. Curry, J. Schramm, E. E. Ebert, Sea ice-albedo feedback mechanism. *J. Climate*, **8**, 240–247 (1995).

17. I. M. Held, B. J. Soden, Robust responses of the hydrological cycle to global warming. *J. Climate* **19**, 5686–5699 (2006).

18. G. A.Vecchi *et al*., Weakening of tropical Pacific atmospheric circulation due to anthropogenic forcing. *Nature* **441**, 73–76 (2006).

19. K. L. Brubaker, D. Entekhabi, Analysis of feedback mechanisms in land-atmosphere interaction. *Water Resource Res*. **32**, 1343–1357 (1996).

20. K.-M. Lau, K-M. Kim K-M, The 2010 Pakistan flood and Russian heat wave: Teleconnection of hydrometeorologic extremes. *J. Hydromet.* **13**, 392–403 (2012). doi:10.1175/JHM-D-11-016.1

21. C. Chou, J. D. Neelin, Mechanisms of global warming impacts on regional tropical precipitation. *J. Climatol.* **17**, 2688–2701 (2004). doi:10.1175/1520

22. C. Chou, J. D. Neelin, C. A. Chen, J. Y. Tu, Evaluating the "rich-get-richer" mechanism in tropical precipitation change under global warming, *J. Clim.* **22**, 1982–2005 (2009). doi:10.1175/2008JCLI2471.1

23. B. N. Goswami, V. Venugopal. D. Sengupta, M. S. Madhusoodanan, P. K. Xavier, Increasing trend of extreme rain events over Indian in a warming environment. *Science* **314**, 1442–1445 (2006).

24. J. Lu, C. Deser, T. Reichler, Cause of the widening of the tropical belt since 1958, *Geophys. Res. Lett*. **36**, L03803 (2009). doi:10.1029/ 2008GL036076

25. R. Seager *et al*., Model projections of an imminent transition to a more arid climate in southwestern North America. *Science* **316**, 1181–1184 (2007).

26. X. Zhang *et al*., Detection of human influence on twentieth century precipitation trends. *Nature* **448**, 461–465 (2007).

27. R. Koenker, K. Hallock, Quantile regression: an introduction. *J. Economic Perspectives* **15**, 143–156 (2001).

28. L. Hao, D. Q. Naiman, *Quantile Regression*. (Sage Publications, Thousand Oaks, CA, USA, 2007).

29. R. F. Adler et al., The Version 2 Global Precipitation Climatology Project (GPCP) Monthly Precipitation Analysis (1979-Present). *J. Hydrometeor*. **4**, 1147-1167 (2003).

30. G. J. Huffman et al., The TRMM Multi-satellite Precipitation Analysis: Quasi-Global, Multi-Year, Combined-Sensor Precipitation Estimates at Fine Scale. J. Hydrometeor. **8(1)**, 38–55 (2007)